Received: 25 July 2019 | Revised: 24 August 2020 | Accepted: 17 September 2020

IET Image Processing

DOI: 10.1049/ipr2.12082

The Institution of Engineering and Technology WILEY

ORIGINAL RESEARCH PAPER

Single image dehazing based on bright channel prior model and saliency analysis strategy

Libao Zhang | **Shan Wang** | **Xiaohan Wang**

School of Artificial Intelligence, Beijing Normal University, Beijing, People's Republic of China

Correspondence
Libao Zhang, School of Artificial Intelligence, Beijing Normal University, No. 19, XinJieKouWai Street, Beijing 100875, People's Republic of China.
Email: libaozhang@163.com

Abstract

Haze is a common atmospheric phenomenon that causes poor visibility in outdoor images, which greatly limits image application in later stages. Therefore, haze removal has become the first and most indispensable step when dealing with degraded images. In this paper, we propose a novel bright channel prior (BCP) model and a saliency analysis strategy for haze removal. First, we obtain a more robust and accurate atmospheric light by a superpixel-based dark channel method. Second, we utilize the dark channel prior (DCP) to handle dark regions in hazy images. However, the DCP often mistakes white regions for opaque haze and thus causes serious colour distortion and halo effects. To solve this problem, a new BCP is proposed to accurately estimate the transmission of bright regions in hazy images. Third, we fuse the DCP and BCP using a multiscale fusion strategy with Laplacian pyramid representation to gain the correct transmission information for both bright and dark regions. Finally, a novel saliency analysis strategy for transmission refinement is proposed, so that the texture details can remain present to the greatest extent in the restored images. The experimental results illustrate that our proposed method performs well in restoring images containing bright objects.

1 | INTRODUCTION

Haze, a common atmospheric phenomenon that occurs under natural conditions, forms a complex illumination environment that leads to image contrast decline, blurring, colour pollution, and many other issues [1–4]. The deterioration of image quality seriously affects applications of images in computer vision systems, such as target detection, tracking, and autonomous navigation [5]. Thus, haze removal has become a hotspot in the field of image processing.

Existing dehazing methods can be broadly divided into two categories: multiple image-based and single image-based techniques [6]. Methods based on multiple images usually need to obtain multiple images of the same scene under different weather or polarization conditions. Narasimhan et al. [7] presented a physics-based method to restore scene contrast from two weather conditions. The limitation of these methods is that multiple images and additional information are not available all the time, and thus, these dehazing methods can hardly be used in the real world.

In contrast, methods based on a single image only use one hazy image but usually utilize assumptions and priors to solve problems. Fattal et al. [8] removed the haze component by assuming that surface shading and scene transmission are locally uncorrelated. He et al. [9] proposed the dark channel prior (DCP) to estimate the transmission and airlight. Enlightened by DCP, Tarel et al. [10] achieved fast haze removal using median filtering. Meng et al. [11] recovered a high-quality image with fine details based on boundary constraint and contextual regularization. Zhu et al. [12] proposed a colour attenuation prior for single image haze removal. However, the applicability of these methods is still insufficient due to the non-universal assumptions required.

With the development of artificial neural networks [13], data-driven approaches for single image dehazing have become the focus of recent studies. Cai et al. [14] proposed DehazeNet,

which adopted a convolutional neural network architecture to remove haze. Li et al. [15] subsequently presented AOD-Net, a fully end-to-end image dehazing network. However, these data-driven dehazing methods require complex model training and parameter tuning, which lead to high computational complexity and time consumption [16].

In this paper, a simple but effective single-image dehazing method is proposed based on the bright channel prior (BCP) model and a saliency analysis strategy. The major contributions of our paper are as follows.

1. A superpixel-based atmospheric light estimation method is presented in which the superpixel technique is used to generate a dark channel. Experiments show that the superpixel-based dark channel is more accurate and robust than the original dark channel.
2. We propose a BCP on the basis of the observation that in most images with local bright regions there are a multitude of pixels that have very high intensity in at least one colour channel. We then employ a multiscale fusion strategy to automatically combine the advantages of the DCP model and BCP model.
3. We also propose a novel refining approach based on saliency analysis. We first use saliency detection to capture depth change regions; then, the saliency value is used as an adjustable factor to compute proper guidance images in which most of the texture details are blurred but the depth change regions remain clearly visible.

The remainder of this paper is organized as follows. In Section 2, the haze model used to generate hazy images is described. In Section 3, we introduce the theory of the dark channel prior. In Section 4, the proposed dehazing algorithm is introduced in detail. In Section 5, the performance of the proposed method is compared with seven competing methods. In Section 6, the conclusion is drawn.

2 | HAZE MODEL

Generally, the formation of a hazy image can be described as the following model [17, 18]:

$$\mathbf{I}(x) = \mathbf{J}(x)t(x) + \mathbf{A}(1 - t(x)) \tag{1}$$

where x is the pixel coordinate, $\mathbf{I}$ is the observed intensity, $\mathbf{J}$ is the scene radiance, t is the medium transmission and $\mathbf{A}$ is the global atmospheric light. From Equation (1), we can see that the key of recovering haze-free images is to estimate correct transmission t and atmospheric light $\mathbf{A}$ from the input hazy images.

Assuming the atmosphere is homogenous, the transmission t can be further expressed as

$$t(x) = e^{-\beta d(x)} \tag{2}$$

where β is the atmospheric attenuation coefficient, and d is the scene depth. Equation (2) indicates that transmission depends only on scene depth when β remains constant.

3 | DARK CHANNEL PRIOR

He et al. [9] first proposed the concept of DCP. They observed that the minimum intensity of the three channels is close to zero on outdoor haze-free images, and they formulated it as the DCP prior

$$J^{\text{dark}}(x) = \min_{y \in \Omega(x)} \left(\min_{c \in \{r,g,b\}} J^c(y) \right) \to 0 \tag{3}$$

where J^{dark} is the dark channel of $\mathbf{J}$. J^c is a colour channel of $\mathbf{J}$, and $\Omega(x)$ is a local patch centred at x. $c \in \{r, g, b\}$ denotes colour channel index.

On the basis of $J^{\text{dark}}(x) \to 0$, the transmission $t_d(x)$ can be deduced from Equation (1)

$$t_d(x) = 1 - \omega \min_{y \in \Omega(x)} \left(\min_{c \in \{r,g,b\}} \frac{I^c(y)}{A^c} \right) \tag{4}$$

where ω is a constant parameter between 0 and 1 to optionally keep a very small amount of haze for remote objects. This parameter is set to 0.95 in [9].

4 | THE PROPOSED METHOD

The proposed method for restoring hazy images is introduced in this section. Based on the haze model, we first estimate atmospheric light using the superpixel-based dark channel technique. Second, to restore the white regions that do not satisfy the DCP, we propose the BCP model. Then a multiscale fusion strategy is imposed to estimate the rough transmission map. Subsequently, a proper guidance image is generated based on saliency analysis for further transmission refinement. Finally, the hazy image is restored by the previously described haze model. The complete flowchart of the dehazing algorithm is shown in Figure 1.

4.1 | Superpixel-based atmospheric light estimation

In conventional studies, most dehazing methods use the brightest pixel in a single hazy image to represent atmospheric light, which neglects saturated pixels, especially pixels in the white object regions. To minimize the influence of the above issue on atmospheric light estimation, He et al. [9] estimated atmospheric light by picking the top 0.1 percent of brightest pixels in the dark channel. However, for complex scenes, the method using local patches may still misestimate atmospheric light.

To solve the above problem, we propose a superpixel-based dark channel computation method that can effectively reduce the influence of white objects on atmospheric light estimation. We utilize superpixels instead of local patches to construct the dark channel. This method is more robust and accurate than the local patch-based method since the superpixels combine adjacent pixels with similar texture, colour, brightness and other characteristics into one region. In this paper, we use the SLIC algorithm [19] to segment the minimum channel image

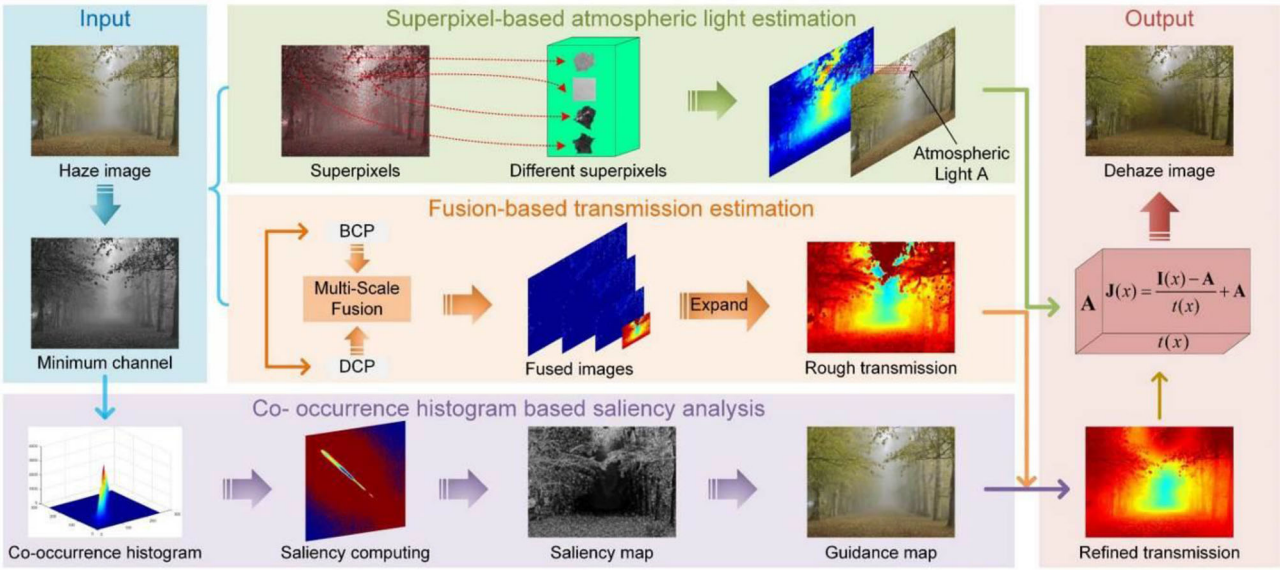

FIGURE 1 Framework of our proposed model

$M(x)$ into superpixels $\{g_1, g_2, g_3, \ldots, g_N\}$, where N is the number of superpixels. Then the superpixel-based dark channel can be formulated as

$$M(x) = \min_{c\in\{r,g,b\}} J^c(x) \tag{5}$$

$$J^{\text{superdark}}(x) = \min_{y\in g_i}(M(y)), i = 1, 2, \ldots, N. \tag{6}$$

Based on the superpixel-based dark channel, we pick the top 0.1 percent of brightest pixels from $J^{\text{superdark}}(x)$. Then the corresponding pixels with the highest intensity in the hazy image among these pixels are chosen as atmospheric light.

4.2 | Fusion-based transmission estimation

In addition to the atmospheric light, the key of recovering haze-free images is to estimate correct transmission. However, many estimation methods are not very effective in specific cases, especially when hazy images contain large bright regions. Therefore, we introduce a novel method to improve transmission estimation accuracy. We also employ a classical multiscale fusion strategy to automatically combine the advantages of the DCP and our proposed BCP model.

4.2.1 | Bright channel prior

BCP is proposed in our method to handle bright regions in hazy images. Unlike the DCP [9], in bright regions, pixels have a very high intensity in at least one colour channel, which can be described as

$$J^{bright}(x) = \max_{y\in\Omega(x)}\left(\max_{c\in\{r,g,b\}} J^c(y)\right) \to 1 \tag{7}$$

where $J^{bright}(x)$ denotes the bright channel. Then, we normalize Equation (1) into

$$\frac{I^c(x)}{A^c} = t(x)\frac{J^c(x)}{A^c} + 1 - t(x) \tag{8}$$

where I^c is a colour channel of $\mathbf{I}$, and A^c is a colour channel of $\mathbf{A}$. Assuming that the transmission computed by BCP is constant in a local patch [9], we can calculate the bright channel on both sides of Equation (8)

$$\max_{y\in\Omega(x)}\left(\max_{c\in\{r,g,b\}}\frac{I^c(y)}{A^c}\right) = t_b(x)\max_{y\in\Omega(x)}\left(\max_{c\in\{r,g,b\}}\frac{J^c(y)}{A^c}\right) + 1 - t_b(x) \tag{9}$$

where $t_b(x)$ is the patch's transmission based on the BCP. According to [30], the values of atmospheric light are generally close to those of the brightest pixels in a hazy image, and the intensity values of the RGB channels are approximately equal. Therefore, we use the mean value of the RGB channels as the atmospheric light in this paper

$$A = \frac{1}{3}\sum_{c\in\{r,g,b\}} A^c \tag{10}$$

Thus, Equation (9) can be further expressed as

$$\frac{\max_{y\in\Omega(x)}\left(\max_{c\in\{r,g,b\}} I^c(y)\right)}{A} = \frac{t_b(x)\max_{y\in\Omega(x)}\left(\max_{c\in\{r,g,b\}} J^c(y)\right)}{A} + 1 - t_b(x) \tag{11}$$

Putting Equation (7) into Equation (11), we can estimate the transmission $t_b(x)$ by

$$t_b(x) = \frac{\max\limits_{y\in\Omega(x)}\left(\max\limits_{c\in\{r,g,b\}} I^c(y)\right) - A}{1-A} \tag{12}$$

Because the BCP is not good prior for dark regions, it may cause $t_b(x) < 0$. Therefore, we take the maximum value among $t_b(x)$ and 0.05

$$t_b(x) = \max(t_b(x), 0.05) \tag{13}$$

In contrast, the transmission map $t_d(x)$ for dark regions can be estimated by the DCP [9] using Equation (4). According to the transmission maps $t_b(x)$ and $t_d(x)$, we can obtain the correct scene radiances for bright and dark regions, respectively.

4.2.2 | Multi-scale fusion

As described, the two different transmission maps obtained above are complementary. In other words, they are equally important. Therefore, one natural idea is to combine the complementary information using an image fusion method to achieve a new fused image that contains the best information from the two original images.

Therefore, we adopt a multiscale fusion strategy using Laplacian pyramid representation [20] to combine the two different transmission maps. In our case, the two transmission maps $t_b(x)$ and $t_d(x)$ are decomposed into L-level pyramids through the Laplacian pyramid decomposition method [21]. Then, we fuse each level of the Laplacian pyramid by

$$LP_l^f(x) = \max\left\{LP_l^b(x), LP_l^d(x)\right\} \tag{14}$$

where l is the lth level Laplacian pyramid ($0 < l \le$ L), and LP_l^f is the fused result. LP_l^b and LP_l^d are the Laplacian versions of $t_b(x)$ and $t_d(x)$, respectively. Finally, the fused transmission map $t(x)$ is obtained by the inverse Laplacian pyramid transform.

$$t(x) = \sum_l \underset{2^{l-1}}{expand}(LP_l^f(x)) \tag{15}$$

where $\underset{2^{l-1}}{expand}(\cdot)$ is the upsampling operation, which can expand the image 2^{l-1} times. In this paper, L is set to 4.

4.3 | Saliency-based guidance image generation

After roughly estimating the primary transmission map, the next step is to refine it. In general, the guided image filter (GIF) [22], a filter that transfers the structure of the guidance image to the filtering output, is used for further refinement.

Traditionally, most dehazing methods directly use hazy images as guidance images. However, the drawback of these methods is that the refined transmission maps and the hazy images will have fairly similar texture details. In other words, the change in the transmission is mostly determined by the hazy image, which goes against the principle that transmission only depends on scene depth. Thus, haze-free images will suffer from a great loss of texture detail.

In this paper, saliency analysis is proposed to solve the above problem. First, we use the co-occurrence histogram-based saliency detection method to capture the regions of depth change and then to generate a saliency map. Finally, the saliency map is utilized as a coefficient matrix to produce a proper guidance image.

4.3.1 | Co-occurrence histogram

The co-occurrence histogram is a two-dimensional joint distribution of image values that is capable of capturing the global and local distributions of intensity values. Thus, it can be used as a good measure to calculate visual saliency [31].

Given a single channel image I_m with k grey levels, the co-occurrence matrix COH can be defined as

$$COH = [coh(m,n)],\ m,n \in IK \tag{16}$$

where COH is a symmetric square matrix of size $k \times k$. $IK = \{1, 2, 3, \ldots, k\}$ is a set of k possible image values within I_m. A COH element $coh(m,n)$ can be computed as follows: Both m and n denote pixel values. For each $I_m(i,j) = m$, where (i,j) is a coordinate, we count the number of pixels with a value of n in the local patch Ω_ζ of size $\zeta \times \zeta$ centred at (i,j) (ζ is set to 3 in this paper). Then, $coh(m,n)$ is the sum of all these numbers.

4.3.2 | Co-occurrence histogram-based saliency map generation

As has been stated before, haze severely degrades image colour and causes the loss of detailed texture information. Moreover, the clarity of a hazy image is directly related to the thickness of the haze, which depends on the scene depth. In other words, objects with the same scene depth generally have similar clarity in a hazy image. As in previous studies [23, 24], the depth change regions are decided by the occurrence frequency of pixel pairs, i.e., the depth region occurs as pixel pairs that have low occurrence frequencies. Based on this idea, we propose the co-occurrence histogram-based saliency detection method to capture depth information, in which a high saliency value represents depth change regions, i.e., pixel pairs that have low occurrence frequencies.

For each pixel, the minimum value in the RGB channel is the upper limit of the haze thickness of the pixel [9]. Therefore, to accurately obtain depth change regions, the minimum channel image, generated by calculating the minimum value in the RGB channel for each pixel, is used to compute the saliency map.

For the convenience of the follow-up calculation, the co-occurrence matrix COH is normalized by its maximum element

$$NCOH = [ncoh(m, n)] = \frac{COH}{\max(COH)} \tag{17}$$

where $NCOH$ is the normalized co-occurrence matrix.

As mentioned, pixel pairs that rarely appear should have high saliency values; thus, we first compute the primary saliency value of each intensity pair by

$$s(m, n) = \begin{cases} -\ln(ncoh(m, n)), & ncoh(m, n) > 0 \\ 0, & otherwise \end{cases} \tag{18}$$

where $s(m, n)$ denotes the saliency value of the intensity pair of m and n. Finally, the saliency map of the input image can be obtained by computing $Sa(i, j)$

$$Sa(i, j) = \sum_{i'=i-r}^{i+r} \sum_{j'=j-r}^{j+r} s(I_m(i, j), I_m(i', j')) \tag{19}$$

where $Sa(i, j)$ is the saliency value of each input pixel and r is the window radius that is used in computing each element of $NCOH$.

4.3.3 | Coefficient fusion-based guidance image generation

In this paper, the input hazy image is used as one guidance image G_1, which can retain abundant texture information. In contrast, the other smoothing guidance image G_2 can be obtained by performing an average filter on G_1. Therefore, our task is to seek an optimal combination of the two different guidance images.

As mentioned above, the saliency map can partly represent the change in image depth; thus, the saliency map Sa is used as a coefficient to fuse G_1 and G_2 in this paper. However, the saliency map only focuses on the edges but ignores the pixels near these edges. Since these pixels are in the windows that also contain depth changes, they should also assign a greater weight to G_1 rather than to G_2. Therefore, a refined adjustable factor $F(x)$, which is related to the distance between two-pixel coordinates x and y, is defined as

$$F(x) = \max_{y \in \Omega(x)} \frac{Sa(y)}{d(x, y) + 1} \tag{20}$$

$$d(x, y) = \frac{E(x, y)}{\sigma} \tag{21}$$

where $E(x, y)$ is the Euclidean distance between x and y, and σ is the window radius of the average filter. The final guidance image $G(x)$ can be obtained by

$$G(x) = F(x) * G_1 + (1 - F(x)) * G_2 \tag{22}$$

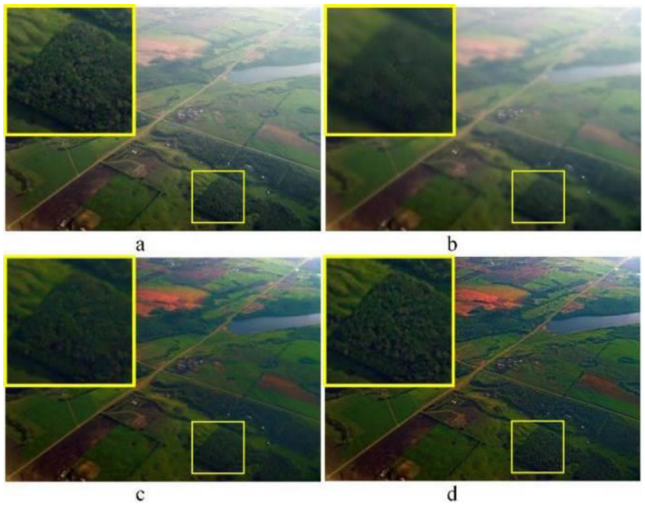

FIGURE 2 Different guidance images and their corresponding results. (a) Input image (common guidance image); (b) our guidance image. (c) Haze-free image recovered by (a); (d) haze-free image recovered by (b)

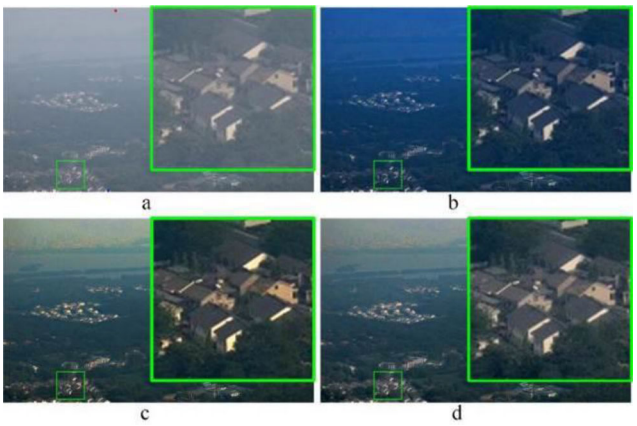

FIGURE 3 Comparison between the original dark channel and the superpixel-based dark channel for atmospheric light. (a) Hazy images in which the red point is the atmospheric light obtained using the proposed method, while the blue point is the atmospheric light obtained using He's method. (b) Dehazing results obtained using He's method. (c) Dehazing results obtained using the superpixel-based dark channel and He's method. (d) Dehazing results using the proposed method

Therefore, the refined transmission map $t_r(x)$ can be calculated by

$$t_r(x) = GIF\{t(x), G(x)\} \tag{23}$$

where $GIF\{\cdot\}$ denotes the GIF operator [22].

Figure 2 gives an example of a common guidance image and our guidance image, and their corresponding dehazing results. Comparatively, our guidance image contributes more abundant and natural details than the common guidance image.

5 | EXPERIMENTAL RESULTS

In our experiment, we evaluate the effectiveness of the proposed method by performing both qualitative and

FIGURE 4 Testing hazy images in the Middlebury Stereo dataset

quantitative analyses on the synthetic hazy dataset and real-world hazy images. The conventional comparison algorithms include the DCP (TPAMI'10) [9], NLD (CVPR'16) [25], DCPEM (SPL'18) [26], RAT (JEI'18) [6] and AMEF (SP'18) [28]. The learning-based comparison methods are DehazeNet (TIP'16) [14] and MSCNN (ECCV'16) [27]. The experimental codes are run on MATLAB R2017a.

5.1 | Comparison of atmospheric light

The comparison of the original dark channel and the superpixel-based dark channel for atmospheric light is shown in Figure 3. In Figure 3(a), the red point is the atmospheric light estimated by the proposed method, while the blue point is the atmospheric light estimated by He's method. Obviously, He's method mistakenly regards the white regions as the most haze-opaque regions by using the original DCP. Figure 3(b) shows the dehazing results using the original dark channel method, which have serious colour distortion and are oversaturated. If the superpixel-based dark channel is used to estimate atmospheric light in He's dehazing method, as shown in Figure 3(c), it helps to restore the hazy image. However, the results are still oversaturated. Figure 3(d) shows the dehazing results using the proposed method. From the results, we can see that there is a major improvement in the recovery of hazy images.

5.2 | Quantitative comparison

As stated in [29], most dehazing algorithms rely on the full-reference peak signal-to-noise ratio (PSNR) and the structural similarity (SSIM) metrics, with assuming a synthetic testing set with known clean ground truth. In addition, there are many dehazing methods that use PSNR and SSIM as performance measures [2, 14, 15, 26, 27]. Therefore, we also adopt the PSNR and SSIM [32] assessments as comparison indexes to evaluate our proposed method

$$\mathrm{PSNR} = 10 \times \log_{10}\left[\frac{255^2}{MSE}\right] \tag{24}$$

$$MSE(J,J^*) = \frac{1}{wh}\sum_{i=0}^{w-1}\sum_{j=0}^{h-1}\left|J - J^*\right|^2 \tag{25}$$

TABLE 1 Average PSNR and SSIM values on Middlebury Stereo dataset

Model	PSNR (dB)	SSIM
DCP [9]	15.13	0.7956
NLD [25]	14.15	0.6887
DCPEM [26]	15.73	0.8171
RAT [6]	13.73	0.6933
AMEF [28]	15.42	0.8009
DehazeNet [14]	14.67	0.8124
MSCNN [27]	14.75	0.7900
Ours	**15.96**	**0.8287**

Note: The boldface indicates the best performance.
Abbreviations: DCP, dark channel prior; PSNR, peak signal-to-noise ratio; SSIM, structural similarity.

$$\mathrm{SSIM} = \frac{(2\mu_1\mu_2 + C_1)(2\sigma_{12} + C_2)}{(\mu_1^2 + \mu_2^2 + C_1)(\sigma_1^2 + \sigma_2^2 + C_2)} \tag{26}$$

where J and J^* denote the restored image and corresponding reference image, respectively. w and h are the width and height of J, respectively. μ_1 and μ_2 are the means of J and J^*, respectively. σ_1 and σ_2 denote the standard deviations of J and J^*, respectively. σ_{12} is the covariance between J and J^*.

For PSNR, the more similarity there is between the restored image and ground-truth image, the higher the PSNR values are. SSIM is used to evaluate the structural similarity between the two images. A good dehazing algorithm should remove haze as much as possible while preserving the image structure. Therefore, the higher the SSIM value between the dehazed image and the corresponding ground-truth image, the better the performance is.

To prove the superiority of our method in dealing with hazy images containing white objects, we select 12 images from the Middlebury Stereo dataset, most of which contain white backgrounds or objects, as shown in Figure 4. The average PSNR and SSIM values are tabulated in Table 1. Our proposed method achieves the highest PSNR value, mainly because the proposed BCP is better able to handle the bright regions in hazy images. In addition, our SSIM value is also the best. The reason behind this is that the use of saliency-based guidance images can greatly refine the rough transmission map by ensuring that detailed texture information is preserved in the dehazed results.

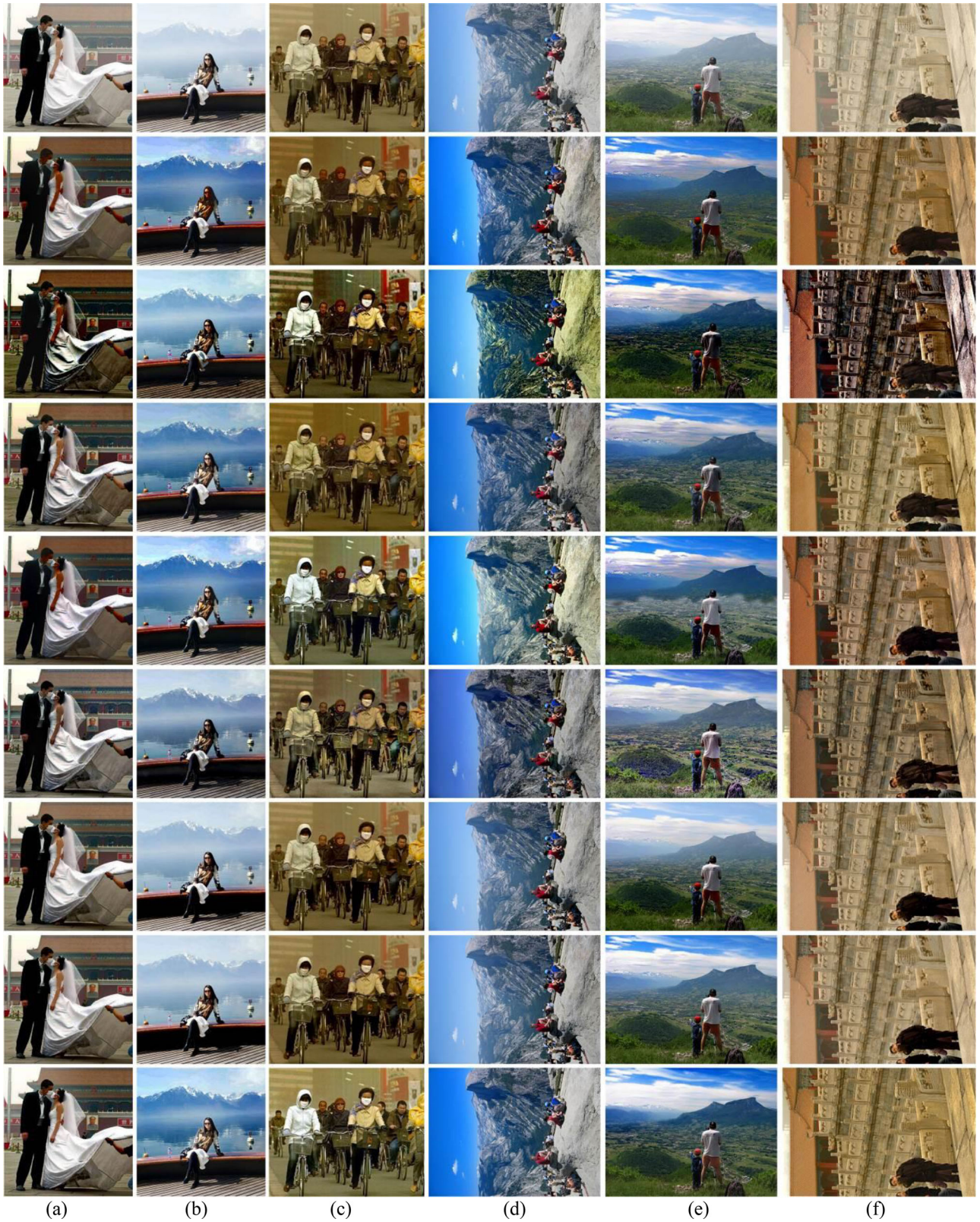

FIGURE 5 Hazy images with white objects and the dehazing results. Haze images (first row), DCP [9] (second row), NLD [25] (third row), DCPEM [26] (fourth row), RAT [6] (fifth row), AMEF [28] (sixth row), DehazeNet [14] (seventh row), MSCNN [27] (eighth row) and the proposed method (the last row). (a) Couple, (b)Woman, (c) Bikes, (d) Yosemite, (e) Man and (f) Gugong1. DCP, dark channel prior.

FIGURE 6 Hazy images without white objects and the dehazing results. Haze images (first row), DCP [9] (second row), NLD [25] (third row), DCPEM [26] (fourth row), RAT [6] (fifth row), AMEF [28] (sixth row), DehazeNet [14] (seventh row), MSCNN [27] (eighth row) and the proposed method (the last row). (a) Gugong2, (b) City, (c) Pumpkins, (d) Wheat, (e) Farm and (f) Leaves. DCP, dark channel prior.

5.3 | Qualitative comparison

The results of different dehazing methods are shown in Figures 5 and 6. The hazy images in Figure 5 all contain white objects, while the hazy images in Figure 6 do not contain white objects. As shown in Figure 5, the DCP [9] usually mistakes the white region for opaque haze, resulting in serious colour distortion and noise in the white object regions, such as with the dress in the second row of Figure 5(a) and with the T-shirt in the second row of Figure 5(e). In addition, NLD [25] generates many fake edges, especially in the third row of Figure 5(a) and (f). DCPEM [26] performs well for some of the images, such as in the fourth row of Figure 5(b), (d) and (f). However, other restored images of DCPEM tend to be oversaturated in

the white regions. RAT [6] performs well on the white regions but badly on other regions, such as the skin and mountain in the fifth row of Figure 5(a) and (e). AMEF [28] has the same problem. By contrast, the two learning-based methods and our proposed method can properly handle hazy images with white regions.

In Figure 6, it can be observed that the proposed dehazing method outperforms the competing methods in terms of colour fidelity and abundance of details. In particular, there are serious halo artefacts in the results of the NLD [25], RAT [6] and AMEF [28] models. In other words, our proposed method is better than the conventional algorithms and achieves a competitive performance compared to the learning-based method.

6 | CONCLUSION

In this paper, we propose a novel single image dehazing method based on the BCP and saliency analysis. Our method can be performed with three steps. In the atmospheric light estimation step, a superpixel-based atmospheric light estimation method is proposed that can effectively improve the accuracy of atmospheric light estimation. In the transmission estimation step, we first propose the BCP model based on our observation to handle bright regions in the hazy images. A fusion-based transmission estimation method is then presented to automatically combine the DCP and BCP models. Finally, we use saliency analysis to refine the rough transmission in the refinement step. Experiments on the synthetic hazy dataset and real-world hazy images demonstrate the effectiveness of the proposed algorithm.

ACKNOWLEDGEMENTS

This work was supported by the Beijing Natural Science Foundation (BNSF) (L182029), the National Natural Science Foundation of China (NSFC) (41771407, 61571050), and the BNU Interdisciplinary Research Foundation for the First-Year Doctoral Candidates under Grant No. BNUXKJC2023.

REFERENCES

1. Liu, P.J., et al.: Contrast in haze removal: Configurable contrast enhancement model based on dark channel prior. IEEE Trans. Image Process. 28(5), 2212–2227 (2018)
2. Liu, R., et al.: Robust haze removal via joint deep transmission and scene propagation. Proceeding of IEEE International Conference on Acoustics, Speech and Signal Processing, Calgary, AB, Canada, pp. 1373–1377 (2018)
3. Kratz, L., Nishino, K.: Factorizing scene albedo and depth from a single foggy image. Proceeding of IEEE International Conference on Computer Vision, Kyoto, Japan, pp. 1701–1708 (2009)
4. Shi, L.F., et al.: Removing haze particles from single image via exponential inference with support vector data description. IEEE Trans. Multimedia. 20(9), 2503–2512 (2018)
5. Guo, J.M., et al.: An efficient fusion-based defogging. IEEE Trans. Image Process. 26(9), 4217–4228 (2017)
6. Zhang, L., et al.: Saliency-driven single image haze removal method based on reliable airlight and transmission. J. Electron. Imaging 27(2), 1 (2018)
7. Narasimhan, S.G., Nayar, S.K.: Contrast restoration of weather degraded images. IEEE Trans. Pattern Anal. Mach. Intell. 25(6), 713–724 (2003)
8. Fattal, R.: Single image dehazing. ACM Trans. Graph. 27(3), 1–9 (2008)
9. He, K., et al.: Single image haze removal using dark channel prior. IEEE Trans. Pattern Anal. Mach. Intell. 33(12), 2341–2353 (2010)
10. Tarel, J.P., Hautiere, N.: Fast visibility restoration from a single color or gray level image. Proceeding of IEEE International Conference on Computer Vision, Kyoto, Japan, pp. 2201–2208 (2009)
11. Meng, G., et al.: Efficient image dehazing with boundary constraint and contextual regularization. Proceeding on IEEE International Conference on Computer Vision, Sydney, Australia, pp. 617–624 (2013)
12. Zhu, Q., et al.: A fast single image haze removal algorithm using color attenuation prior. IEEE Trans. Image Process. 24(11), 3522–3533 (2015)
13. Swami, K., Das, S.K.: CANDY: Conditional adversarial networks based end-to-end system for single image haze removal. Proceeding on IEEE International Conference on Pattern Recognition, Beijing, China, pp. 3061–3067 (2018)
14. Cai, B., et al.: Dehazenet: An end-to-end system for single image haze removal. IEEE Trans. Image Process. 25(11), 5187–5198 (2016)
15. Li, B., et al.: AOD-Net: All-in-one dehazing network. Proceeding on IEEE International Conference on Computer Vision, Venice, Italy, pp. 4770–4778 (2017)
16. Kang, C., Kim, G.: Single image haze removal method using conditional random fields. IEEE Signal Process. Lett. 25(6), 818–822 (2018)
17. Koschmieder, H.: Theorie der horizontalen Sichtweite. Beitr. Phys. Freien Atm. 12, 33–53 (1924)
18. McCartney, E.J.: Optics of the Atmosphere: Scattering by Molecules and Particles. John Wiley and Sons, New York, NY (1975)
19. Achanta, R., et al.: SLIC superpixels compared to state-of-the-art superpixel methods. IEEE Trans. Pattern Anal. Mach. Intell. 34(11), 2274–2282 (2012)
20. Burt, P., Adelson, E.: The Laplacian pyramid as a compact image code. IEEE Trans. Commun. 31(4), 532–540 (1983)
21. Wang, W., Chang, F.: A multi-focus image fusion method based on Laplacian pyramid. J. Comput. 6(12), 2559–2566 (2011)
22. He, K., et al.: Guided image filtering. IEEE Trans. Pattern Anal. Mach. Intell. 35(6), 1397–1409 (2012)
23. Zhang, L., Sun, Q.: Saliency detection and region of interest extraction based on multi-image common saliency analysis in satellite images. Neurocomputing. 283, 150–165 (2018)
24. Zhang, L., Zhang, J.: A new saliency-driven fusion method based on complex wavelet transform for remote sensing images. IEEE Geosci. Remote Sens. Lett. 14(12), 2433–2437 (2017)
25. Berman, D., Avidan, S.: Non-local image dehazing. Proceeding of IEEE Conference on Computer Vision and Pattern Recognition, Las Vegas, USA, pp. 1674–1682 (2016)
26. Zhu, M., et al.: Single image dehazing based on dark channel prior and energy minimization. IEEE Signal Process. Lett. 25(2), 174–178 (2018)
27. Ren, W., et al.: Single image dehazing via multi-scale convolutional neural networks. Proceeding of European Conference on Computer Vision, Springer, Cham, pp. 154–169 (2016)
28. Galdran, A.: Image dehazing by artificial multiple-exposure image fusion. Signal Process 149, 135–147 (2018)
29. Li, B., et al.: Benchmarking single-image dehazing and beyond. IEEE Trans. Image Process. 28(1), 492–505 (2018)
30. Tan, R.T.: Visibility in bad weather from a single image. Proceeding of IEEE Conference on Computer Vision and Pattern Recognition, Anchorage, AK pp. 1–8 (2008)
31. Lu, S., et al.: Robust and efficient saliency modelling from image co-occurrence histograms. IEEE Trans. Pattern Anal. Mach. Intell. 36(1), 195–201 (2014)
32. Wang, Z., et al.: Image quality assessment: From error visibility to structural similarity. IEEE Trans. Image Process. 13, (4), 600–612 (2004)

How to cite this article: Zhang L, Wang S, Wang X. Single image dehazing based on bright channel prior model and saliency analysis strategy. *IET Image Process.* 2021;15:1023-1031.
https://doi.org/10.1049/ipr2.12082